INFLUENCE OF TEM LOW ENERGY ELECTRON IRRADIATION ON InP DAMAGE STRUCTURE IRRADIATED PREVIOUSLY BY 100 keV Au IONS

A. S. Khalil [a,1], *A. Yu. Didyk* [b,2]

[a] Tabbin Metallurgical Institute, Cairo, Egypt

[b] Joint Institute for Nuclear Research, Dubna

The behavior of disordered isolated volumes (zones) in InP under electron action was characterized by TEM observations. The total areal fraction of the disordered zones in initial InP pre-irradiated by 100 keV heavy Au ions decreased as a function of irradiating electron fluence (time of TEM electron beam irradiation) within all the investigated electron energy range (100–300 keV). Disappearance of disordered zones shows that these zones are sensitive to electron beam irradiation and recover even under electron energies not sufficient to directly elastically displace lattice atoms In and P.

Изучено поведение разупорядоченных зон в InP под действием электронов просвечивающего электронного микроскопа (ПЭМ). Суммарная доля разупорядоченных зон уменьшается как функция электронного флюенса (времени облучения на ПЭМ) для всех изученных энергий электронов (100–300 кэВ). Растворение разупорядоченных зон показывает, что эти области чувствительны к облучению электронами и их возврат не может быть объяснен упруго смещенными атомами In и P. Эти процессы могут быть связаны с термическими процессами при облучении электронами на ПЭМ.

PACS: 61.82.Fk, 68.37.Lp

INTRODUCTION

This article is the continuation of the previous one [1] in which the results of radiation effects with creation of damage zone and amorphization of InP semiconductor single crystal samples (SSCS) under irradiation with low energy Au ions (100 keV) were presented. Using of Rutherford Backscattering Technique (RBS) and Transmission Electron Microscope (TEM) damage structure of irradiated InP SSCS versus the ion fluences was studied. Recently, it has been demonstrated that electron irradiation at an energy lower than the threshold energy required to produce direct atomic displacement (point defects) has resulted in zone shrinkage and disappearance in several elemental and compound semiconductors [1, 2]. The disappearance rate of thermally and laser-induced recovery of these zones was compared to the electron beam-induced recovery process, it was found that the electron beam-induced recovery was more efficient (judging by the disappearance rate versus elapsed time) than the first two processes [3]. TEM image computer analysis was used to extract the recovery

---

[1] E-mail: askhalil2004@yahoo.com

[2] E-mail: didyk@jinr.ru

behavior during *in-situ* electron irradiation. Zone diameters, based on approximating of the area of irregular zone morphology to a circle, were reported to shrink linearly with increasing electron fluence, the shrinkage rate falling with decreasing electron energy. The observed shrinkage rate fell to a minimum at electron beam energies corresponding to elastic energy transfers $\sim 0.5 E_d$ (where E_d is the displacement energy assumed to be an *overall average* atomic displacement energy neglecting crystalline directional dependences).

Surprisingly, the shrinkage rate increased again at lower electron energies ($\leqslant 100$ keV) and was found to be insensitive to the crystallographic orientation and the temperature at which the *in-situ* electron irradiation was carried out. These experiments clearly suggest that low energy electron beam recovery may not require point defects production by direct elastic atomic displacement but rather that electron excitation and ionization effects (inelastic) may be responsible for the surprising observations. Recent MD simulations [4] have shown that the process of recovery for amorphous zones in subthreshold electron irradiation of Si might possibly be not only due to the elastic energy transfer but also by inelastic processes involving, for example, bond breakage and a rearrangement of the disrupted atomic order at the amorphous-zone/crystal lattice interface.

The purpose of this article is the study of behavior and evolution of damage zones produced by low energy Au$^+$ ion irradiation of InP semiconductor single crystal (see [1]) and following electron beam-induced disappearance of disordered zones under electron irradiation by TEM electronic microscope.

1. EXPERIMENTAL PROCEDURE

InP samples were prepared for irradiation from a 500 μm thick, semi-insulating, polished, (001) oriented InP wafer. In addition to bulk samples, thin foil samples (electron transparent $\leqslant 200$ nm thick) were prepared before the ion irradiation in order to avoid the artifacts usually associated with post-irradiation preparation of InP and to facilitate the immediate TEM observation of the irradiated samples. Both the bulk and thin foil samples were irradiated by 100 keV Au ions in a non-channelling direction at room temperature using the tandem accelerator at the Electronic Materials Engineering department at the Australian National University (ANU). The Au ion fluence ranged from $1.0 \cdot 10^{12}$–$1.0 \cdot 10^{14}$ cm^{-2} and the ion flux was $\sim 5.7 \cdot 10^{11}$ cm$^{-2} \cdot$ s^{-1} [1]. The TEM *in-situ* electron irradiation of Au ion irradiated samples were observed isolated disordered zones and were performed in Phillips CM-300 microscope (see [1]). The electron irradiations were carried out using the illuminating electron beam as a function of both electron beam energy and fluence. The evolution of disorder under electron beam irradiation was investigated for five different electron beam energies ranging from 100 to 300 keV, thus the electron dosimetries were quantified for the electron beam energies. The beam current was first accurately measured at 300 keV using a Gatan analytical double tilt holder fitted with an electrically isolated Faraday cup. Maximum value of beam current was $i_{\max} = (8.3 \pm 1.6)$ nA. The beam was then spread to cover the circular viewing fluorescent screen at magnifications sufficient to observe and analyze the disordered zones (magnification was about $\times 70000$) and the exposure time which determines the beam intensity falling on the fluorescent screen (at this current) was acquired (as indicated by the exposure meter in the TEM panel). Beam profiles falling on the sample for the other obtained energies (100–300 keV) were plotted to ensure the uniformity of electron flux over the beam widths. The beam diameter at full width half maximum (FWHM) was determined for each beam

energy (steps of 50 keV) and found to be $D \sim 2$ μm. By scaling the exposure times for each energy to that acquired for 300 keV for which an accurate electron beam current has been measured, estimations for beam currents were obtained. Thus, during electron irradiations, the electron beam was spread over a FWHM of ~ 2 μm where the beam has a uniform profile. For each experiment the flux was maintained constant and hence the total electron fluence was proportional to the irradiation time. The electron current density irradiating the samples (J) was in the range $0.1 \leqslant J \leqslant 0.4$ A $\cdot$ cm^{-2}.

The contrast of the observed zones was enhanced by using bright field technique down the $\langle 001 \rangle$ zone axis, where these zones generally appear as irregular dark contrast features in a homogeneous light background. And the *in-situ* electron irradiation was conducted axially along the $\langle 001 \rangle$ zone axis to investigate electron beam-induced recovery of disorder created by 100 keV Au$^+$ ion irradiation of InP. Thus, a field of many disordered zones was identified in an area of the lowest ion fluence irradiated InP sample ($1.0 \cdot 10^{12}$ cm^{-2}) and the evolution of that initial disorder under electron beam irradiation in TEM was *in-situ* monitored. Thus, each *in-situ* TEM observation for particular electron beam energy rendered a series or time sequence of TEM images which enabled us to access the TEM observed recovery of the initial disorder with the irradiating electron fluence for the corresponding electron energy. The images were digitized, computer processed using Adobe Photoshop software to enhance the overall images quality and improve contrast, subsequently. The AnalySiS$^{\circledR}$ software package [5] was used for quantitative image analyses (to estimate the total area of the observed disorder for each image in a sequence). It is relatively straightforward to measure an irregularly shaped feature such as single zone from a digitized image. However, for an image with a field of many irregularly shaped features (disordered zones) of different contrast levels (different gray levels) as obtained in a typical TEM image, difficulties may arise in setting threshold levels for that digitized image for the subsequent computer analysis as the effect of altering the threshold even slightly can be quantitatively large [6]. To find the optimum threshold levels, visually judged by observing the best levels that define and encompass almost all the observed different dark contrast features (zones) for all the images in a particular TEM image sequence, hence, a set of S-shaped graphs for micrographs of each sequence was obtained based upon continuous threshold level variation (the abscissa) and the corresponding calculated total areal fraction of all the dark contrast (the ordinate) versus threshold level values. We found that the optimum threshold levels lie (on the abscissa) at approximately $\sim 50\%$ of the value of the threshold level of the inflection point on the second derivative graphs of these S-shaped graphs. It was found that this delivered the best and maximum definition of all the disordered zone boundaries in the same sequence of TEM images. Hence, this image optimization process was carried out for each series of the obtained TEM images (i.e., for every TEM image sequence of the investigated electron beam energies).

2. RESULTS AND DISCUSSION

The results of radiation zones accumulation under Au (100 keV) irradiation versus fluence and ion energy with the use of TEM and RBS/C analysis and a phenomenological model of core creation are presented in [2] and [7], respectively. In Fig. 1 we show an example of evolution of a field of such disordered zones observed during 200 keV electron irradiation. As evident in the above TEM images, continuous electron irradiation induces shrinkage and
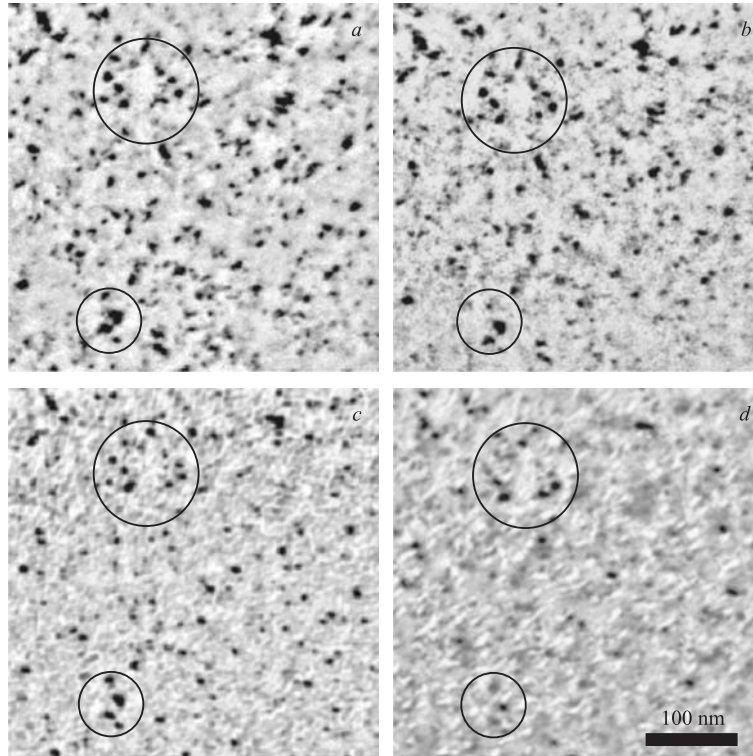
Fig. 1. TEM sequence of *in-situ* observations of disordered zones recovery under 200 keV electron irradiation: before electron irradiation (*a*) and after electron fluence $\sim 0.6 \cdot 10^{22}$ cm^{-2} (*b*), $\sim 1.2 \cdot 10^{22}$ cm^{-2} (*c*) and $\sim 2.2 \cdot 10^{22}$ cm^{-2} (*d*). A couple of clusters of zones are circumscribed with circles

disappearance of disordered zones. For all the investigated electron energies (100–300 keV) the fraction of disorder was found to shrink gradually as a function of increasing electron fluences, where many zones completely disappeared. Quantification of the recovery process of disorder at all electron energies is presented in Fig. 2. In this figure, the total area of all the disorder as the sum of the areas of the observed dark contrast features (zones) normalized to the same initial pre-electron irradiated area (i.e., 0 electron fluence or 0 time) is plotted as a function of the electron fluence. The estimated errors in areal fraction determination (ordinate points) are approximately 5% for each ordinate point as this depends on the optimum threshold level for a micrograph sequence. As apparent from Fig. 2, there is a continual recovery of damage for all the investigated energies.

This is evident as the continuous reduction of the area fraction of disorder where approximately half of the area fraction of disorder recovers following irradiation to electron fluences of $\sim (0.5-1.0) \cdot 10^{22}$ cm^{-2}.

However, an enhanced recovery rate appears for the two lowest energies (100–150 keV), while the recovery is slower for the case of higher energies (200–300 keV). Electron beam-induced recovery is in general a complex process which has been attributed to a wide range of effects [8] mainly to the following:
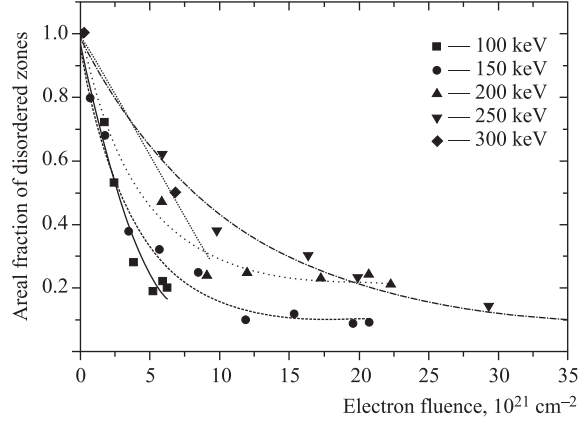
Fig. 2. Areal fraction of disordered zones as a function of electron beam irradiation fluence at various electron beam energies. The uncertainty for each ordinate data point is $\leqslant 5\%$

(1) Direct beam heating, where thermal annealing may be the reason of disappearance of disordered zones.

(2) Elastic interactions and atom knock-ons giving rise to enhanced point defects mobility.

(3) Electronic excitation involving the breaking or rearrangement of unstable bonds.

Let us estimate maximum and average energies which can be transferred to In and P knock-on atoms in elastic collisions of electrons with InP atomic lattice. The maximum $\varepsilon_{\max}$ and average $\varepsilon_{\text{aver}}$ energies of primary knocked atoms (PKA) and inelastic energy loss of electrons are presented in the Table. The calculations of these energies were carried out with the use of computer code developed in [9].

Average energy loss on ionization and excitation was calculated using Rohrlich–Carlson formula [10, 11] which is the relativistic analog of Bethe–Bloch formula [10–12]:

$$-\left(\frac{dE}{dx}\right)_{\text{inel}} = \frac{2\pi e^4 ZN}{mV^2}\left\{\ln\frac{T^2}{\overline{I}^2}\frac{\gamma+1}{2} + 1 - \beta^2 - \frac{2\gamma-1}{\gamma^2}\ln 2 + \frac{1}{8}\left(\frac{\gamma-1}{\gamma}\right)^2 + \delta\right\}, \quad (1)$$

where Z is the charge of lattice atoms. Relativistic factor $\beta = V/c$ and factor γ can be presented in relativistic case as

$$\beta = \left(1 - \frac{1}{(1+T/m_ec^2)^2}\right)^{1/2}, \quad \gamma = (1-\beta^2)^{-1/2}. \quad (2)$$

The maximum transferred energy primary knocked atoms (PKA) can be presented in the form:

$$\varepsilon_{\max} = \frac{2ME(E + 2(m_ec_0^2))}{(m_e + M)^2c_0^2 + 2ME}. \quad (3)$$

$T \equiv E - m_ec^2 = (\gamma - 1)m_ec^2$ is the kinetic energy of electrons in relativistic case at $E > m_ec_0^2$, dimensionless parameter $\varepsilon = T/m_ec^2$; δ is the correction due to density effect. More realistic parameter of collisions between electrons and lattice atoms is average energy of PKA which is expression (6) in [9]. $\overline{I}_{\text{In,P}}$ is an ionization potential of In and P lattice atoms if charges of nuclei satisfy the inequality $13 < Z_{\text{In,P}} < 82$ [13]:

$$\overline{I}_{\text{In,P}} = Z_{\text{In,P}}(9.76 + 58.8Z_{\text{In,P}}^{-1.19}) \text{ eV}. \quad (4)$$

For calculation of electron inelastic energy loss in such compounds as InP we use the Bethe sum rule which can be presented approximately as

$$\left(\frac{dE}{dx}\right)^{\text{InP}}_{\text{inel}} \cong c_{\text{In}} \left(\frac{dE}{dx}\right)^{\text{In}}_{\text{inel}} (\rho_{\text{In}}, Z_{\text{In}}, A_{\text{In}}, \delta_{\text{In}}, \overline{I_{\text{In}}}) + c_{\text{P}} \left(\frac{dE}{dx}\right)^{\text{P}}_{\text{inel}} (\rho_{\text{P}}, Z_{\text{P}}, A_{\text{P}}, \delta_{\text{P}}, \overline{I_{\text{P}}}). \quad (5)$$

The concentrations c_{In} and c_{P} of lattice atoms In and P, respectively, are equal to one another, i.e., $c_{\text{In}} = c_{\text{P}} = 0.5$.

Let us present the figures of maximum (using expression (3)) and average energies (see [9], expression (6)) transferred to primary knocked In and P lattice atoms. The corresponding calculated graphs are presented in Figs. 3 and 4, respectively.

Comparison of maximum and average values of energies transferred to PKA allows us to conclude that there is a big difference between them. The probability of PKA creation with
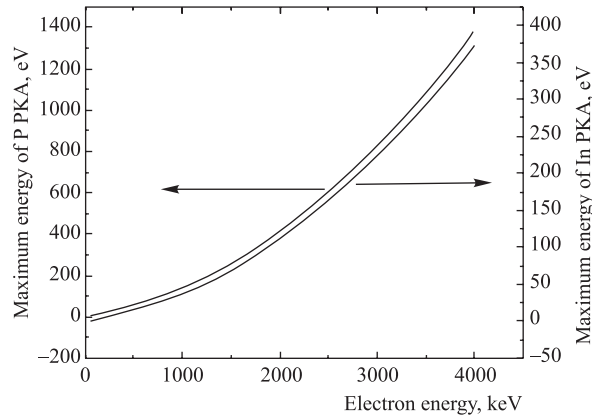

Fig. 3. Dependence of maximum energy transferred to primary knocked In and P atoms (PKA) versus the electron energy
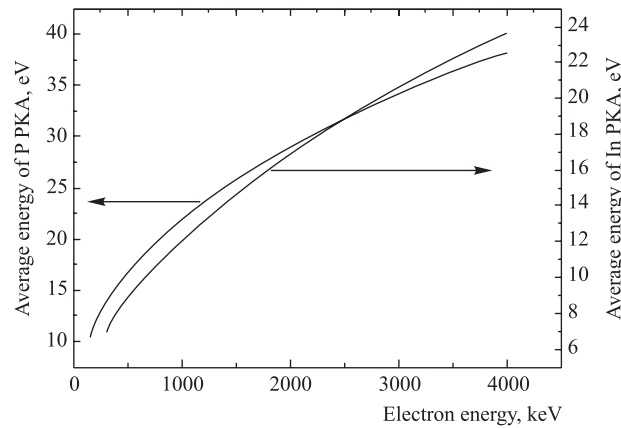

Fig. 4. Dependence of average energy transferred to primary knocked In and P atoms (PKA) versus the electron energy (see [9])

maximum energy $\varepsilon_{\max}$ is very small. So it is necessary to take into account the PKA with average energies. As one can see from expression (6) presented in [9], the calculations of average energy are much better when there exist higher differences between threshold energy of lattice atom displacement (E_{thres}) and maximum transferred energies $\varepsilon_{\max}$. As one can see, the relation between maximum and average energies of PKA is relatively large. Also, in the interval of electron energy 100–300 keV the average energy of PKA may be not enough for creation of displacements in InP.

Now we present the energy dependence of inelastic energy loss (energy loss on ionization and excitation) of electrons in InP (see Fig. 5). This curve was obtained using expressions (1), (2), (4) and (5).

The energies of the electron beams of relevance to our investigations are of course in the range of 100–300 keV and as in Figs. 3 and 4 we presented the relevant interval only for best understanding of such a dependence behavior.

The calculations of temperature rise under electron irradiation in TEM were presented in [2]. The final formula can be expressed as

Fig. 5. Dependence of inelastic energy loss of electrons in InP versus energy of electrons

$$\Delta T_{\text{hole}} = \frac{I_e}{\pi K e} \left(\frac{\partial E}{\partial x}\right)_{\text{inel}} \ln \frac{b}{r_0}, \tag{6}$$

here K, b and r_0 are thermal conductivity (for InP at $T = 300$ K, $K = 0.68$ W/cm/°C [14]), sample for transmission microscope diameter and diameter of the beam, respectively. The temperature rises of InP in comparison with GaP [2] samples under irradiation by electron are presented in the Table.

It is clear that such low values of temperature rise cannot provide the disappearance of disordered zones which was observed at these studies.

The temperature rises in InP and in GaP [2] under electron irradiation for various electron energies at beam current $I_e = 8.3$ **nA**

E, keV	Temperature rise, °C			Beam current, nA
	GaP [2]	$-(\partial E/\partial x)_{\text{inel}}^{\text{InP}}$, keV/nm	InP	
50	0.47	1.772	0.50	8.3
100	0.32	1.139	0.32	8.3
150	0.26	0.910	0.26	8.3
200	0.232	0.793	0.23	8.3
250	0.192	0.723	0.21	8.3
300	0.187	0.677	0.19	8.3

The beam current $i_{\max} = (8.3 \pm 1.6)$ nA corresponds to the following number of electrons per second $N_e^{\max} = i_{\max}/e_0 = (5.2 \pm 1.0) \cdot 10^{10}$ e^-/s on the area of circle with diameter $D = 2$ μm. So the density of electron beam current is $n_e^{\max} = 4N_e^{\max}/\pi D^2 = 1.65 \cdot 10^{18}$ e^-/(s $\cdot$ cm^{-2}). Therefore, for obtaining of electron fluences $(Ft)_1 = 0.6 \cdot 10^{22}$ cm^{-2}, $(Ft)_2 = 1.2 \cdot 10^{22}$ cm^{-2} and $(Ft)_3 = 2.2 \cdot 10^{22}$ cm^{-2}, the necessary time of irradiation was $t_1 = 3.6 \cdot 10^3$ s, $t_2 = 7.2 \cdot 10^3$ s, $t_3 = 1.33 \cdot 10^4$ s, respectively. The time of irradiation is long, so in the irradiation processes one can assume a steady state process.

The thickness of InP TEM samples for the study is about $h = 1000$ Å and diameter of beam circle is $D = 2$ μm. Then, one can conclude that the dissipation of heat from such a thin foil by thermal conductivity processes is very small in distinction of conclusion in [2, 3] (see Eq. (6)). It is necessary to note that the recovery of disordered zones took place only in the area irradiated by electron, there is no any disappearance of disordered zones outside of this circle. The main process of heat dissipation can be the radiation by Stefan–Boltzmann law: $\sigma_{\mathrm{SB}} T^4$.

Let us estimate maximum temperature in the area of electron beam irradiation with the use of simple equation for thermal conductivity:

$$C\rho \frac{\partial T}{\partial t} = \frac{1}{r}\frac{\partial}{\partial r}\left[rK\frac{\partial T}{\partial r}\right] + \left(-\frac{\partial E}{\partial x}\right)_{\mathrm{inel}} n_e^{\max} - 2\sigma_{\mathrm{SB}} T^4 \frac{1}{h}. \tag{7}$$

Here $C = 0.3$ J/(g $\cdot$ K) is the specific capacity of InP at $T = 300$ K and this value has a saturation at $T > 300$ K, m is the mass of a cylindrical volume of InP with the sizes equal to the diameter of the electron beam $D = 2$ μm and height $h \approx 1000$ Å, $K = 0.68$ W/(cm $\cdot$ °C) is the thermal conductivity of InP at $T = 300$ K. The Stefan–Boltzmann constant has a value for absolutely black body:

$$\sigma_{\mathrm{SB}} = 5.6697 \cdot 10^{-12} \ \mathrm{W}/(\mathrm{cm}^2 \cdot \mathrm{K}^4).$$

The irradiation with the use of the Stefan–Boltzmann law can be from both surfaces and also it may be more correct to write such a member in boundary conditions like these:

$$K\frac{\partial T}{\partial x}(x = 0) = a\sigma_{\mathrm{SB}}[T^4(x = 0) - T_0^4],$$
$$K\frac{\partial T}{\partial x}(x = h) = a\sigma_{\mathrm{SB}}[T^4(x = h) - T_0^4]. \tag{8}$$

Here T_0 is the initial temperature of sample, coefficient a is the degree of blackness and $a \leqslant 1$.

The thermal conductivity of InP decreases very quickly with the growth of temperature [14]. Let us consider steady state and also neglect the thermal conductivity term. So one can obtain the simple expression:

$$\left(-\frac{\partial E}{\partial x}\right)_{\mathrm{inel}} hN_e^{\max} - 2\sigma_{\mathrm{SB}}[T^4 - T_0^4]\frac{\pi D^2}{4} = 0. \tag{9}$$

From this expression one can get a value of temperature:

$$T \approx 1.17 \cdot 10^3 \ \mathrm{K}.$$

CONCLUSION

Electron beam-induced recovery of zones was observed *in-situ* in InP as a function of electron energies and fluences. Zones were found to be sensitive to irradiating electrons where they shrink and disappear even at *subthreshold* electron energies (insufficient to displace either the P or In atoms in InP). An important role for inelastic mechanisms in the recovery process is strongly implied. And it appears unnecessary to suppose that only elastically produced Frenkel pairs induce recovery. It is more likely that electron beam-induced ionization (electronic excitation) may play a significant role in the solid-phase recovery process of disorder in InP. The shrinkage and disappearance of zones by electron beam irradiation does not depend on the zone size which might not be singly activated process as the case for recovery of planar amorphous interface.

REFERENCES

1. *Khalil A. S., Didyk A. Yu.* RBS and TEM Studies of Indium Phosphide Irradiated with 100 keV Au Ions // Part. Nucl., Lett. 2009, No. 5 (in press).

2. *Jencic I. et al.* Electron Beam-Induced Crystallization of Isolated Amorphous Regions in Si, Ge, GaP and GaAs // J. Appl. Phys. 1995. V. 78, No. 2. P. 974–982.

3. *Jencic I., Robertson I. M.* Low-Energy Electron Beam-Induced Regrowth of Isolated Amorphous Zones in Si and Ge // J. Materials Res. 1996. V. 11, No. 9. P. 2152–2157.

4. *Frantz J. et al.* Mechanism of Electron-Irradiation-Induced Recrystallization in Si // Phys. Rev. B. 2001. V. 64, No. 12. Art. No. 125313.

5. AnalySIS$^{\textregistered}$, Soft Imaging System. http://www.soft-imaging.net

6. *Russ J. C.* Computer-Assisted Microscopy: The Measurement and Analysis of Images. N. Y.: Plenum, 1990.

7. *Didyk A. Yu., Varichenko V. S.* Track Structure in Dielectric and Semiconductor Single Crystals Irradiated by Heavy Ions with High Level Inelastic Energy Losses // Nucl. Tracks and Rad. Meas. 1995. V. 25, No. 1–4. P. 119–124.

8. *Hobbs L. W.* Radiation Damage with Biological Specimens and Organic Materials // Introduction to Analytical Electron Microscopy / Eds.: J. J. Hern, I. J. I. Goldstein, and D. C. Joy. N. Y., 1979.

9. *Didyk A. Yu., Kozlov O. S., Hofman A.* Calculations of Parameters Characterizing Damage Creation in Materials Irradiated by Relativistic Electrons // Phys. Chem. Material Treat. 2008. No. 1. P. 5–8.

10. *Rohrlich F., Carlson B.* Positron–Electron Differences in Energy Loss and Multiple Scattering // Phys. Rev. 1954. V. 93, No. 1. P. 38.

11. *Boiko V. I. et al.* Interaction of Impulse Charge Particle Beams with Matter. M.: Fizmatlit, 2003. 287 p. (in Russian).

12. *Berthe H. A.* // Proc. Roy. Soc. A (London). 1935. V. 150.

13. *Kononov B. A.* Defect Studies by Swift Electrons. M.: Atomizdat, 1979. 50 p.

14. http://www.ioffe.rssi.ru/SVA/NSM/Semicond/InP/thermal.html